J. Phys.: Condens. Matter **20** (2008) 485215 (12pp) doi:10.1088/0953-8984/20/48/485215

Modelling of strain fields in quantum wires with continuum methods and molecular statics

J J Ramsey[1], E Pan[1] and P W Chung[2]

[1] University of Akron, Department of Civil Engineering and Department of Applied Mathematics, 302 E Buchtel Mall, Akron, OH 44325, USA
[2] US Army Research Laboratory, Aberdeen Proving Ground, MD 21005, USA

E-mail: jjr19@uakron.edu, pan2@uakron.edu and pchung@arl.army.mil

Received 2 September 2008, in final form 6 October 2008
Published 28 October 2008
Online at stacks.iop.org/JPhysCM/20/485215

Abstract
The maximum and minimum principal strains of an InAs quantum wire (QWR) buried in a GaAs matrix are computed using the boundary element method (BEM), the inclusion method, and molecular statics, and the results from each method are compared with each other. The first two methods are based on continuum mechanics and linear elasticity, while the third is atomistic. The maximum principal strains are largely in agreement among the different methods, especially outside the QWR, though in the centre of the QWR, the discrepancy between the continuum and atomistic methods can be as large as 11.9%. The gradients of the strain tensor are in agreement among the methods. The inclusion method is faster than the BEM, and both continuum methods are an order of magnitude faster than molecular statics. Although the inclusion method, unlike the BEM, ignores the difference in material properties between the QWR and its surrounding matrix, its results are in better agreement with the molecular statics results than the results from the BEM. The rough quantitative and qualitative agreements indicate the utility of classical continuum methods for estimating strain profiles in nanoscale structures.

(Some figures in this article are in colour only in the electronic version)

1. Introduction

Although quantum dots (QDs) and quantum wires (QWRs) are small enough for their dimensions to be on the order of the de Broglie wavelength of an electron [1], they can still be large enough to be expensive to model with completely atomistic methods, such as molecular dynamics or molecular statics. Atomistic models typically require millions of particles [2, 3]. The length scale of QD interactions suggests the characteristic length of elastic fields is significantly larger than interatomic spacings, as also evidenced in studies of strains in coherent nanostructures [4]. Therefore, atomistic resolution throughout the entire model is often unnecessary when computing strains, and continuum-based methods offer a relatively computationally inexpensive means to compute such quantities. However, the small dimensions of QDs and QWRs mean that the validity of continuum models of QWRs cannot be taken for granted.

In this paper, the maximum and minimum principal strains of an infinitely long QWR are determined using molecular statics with the Tersoff potential, described in section 2, and also by two different continuum methods: a boundary element method (BEM) described in [5], and an inclusion method described in [6] and [7]. The QWR is shown in cross-section in figure 1. The square QWR is InAs, and the matrix in which it is embedded is GaAs. The QWR is assumed to be in a plane strain state. The Miller index of the xz-plane is (010), where the y-coordinate points into the plane of the page. The origin of the coordinate system is in the centre of the unit cell. The lattice constant of GaAs is given as $a = 0.565\,33$ nm [8]. Such a QWR has been analysed with continuum methods before [6], but not with atomistic methods. An older study in 1998 [9] compared continuum and atomistic approaches as applied to a QD, using the Keating potential [10, 11] for its atomistic calculations and low-order finite difference methods to determine numerical results from its continuum

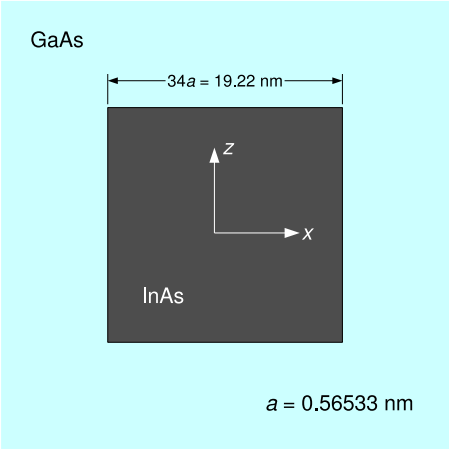

Figure 1. Cross-section of a square QWR embedded in an infinite matrix, where $a = 0.565\,33$ nm is the lattice constant of GaAs.

models. The Keating potential, though, was formulated for small displacements [10], and when Kikuchi *et al* [12] applied it to QDs, they found that it could produce unphysical wavy stress profiles in the substrate beneath the QD.

2. Molecular statics

In molecular statics, the positions of the atoms in the simulation are adjusted in order to minimize the potential energy V. Here, the functional form of the energy is taken to be the empirical Tersoff potential [13, 14],

$$V = \tfrac{1}{2}\sum_{i=1}^{M}\sum_{i\neq j}^{M} f_c(r_{ij})[A_{ij}\exp(-\lambda_{ij}r_{ij}) - b_{ij}B_{ij}\exp(-\mu_{ij}r_{ij})], \quad (1)$$

where M is the number of atoms in the simulation and r_{ij} is the distance between atoms i and j. Other terms in (1) are as follows.

$$f_c(r_{ij}) = \begin{cases} 1 & r_{ij} \leqslant R_{ij} - D_{ij} \\ \tfrac{1}{2}\left\{1 - \sin\left[\pi(r_{ij} - R_{ij})/2D_{ij}\right]\right\} & |r_{ij} - R_{ij}| \leqslant D_{ij} \\ 0 & r_{ij} \geqslant R_{ij} + D_{ij} \end{cases}, \quad (2)$$

$$b_{ij} = \left[1 + (\beta_{ij}\zeta_{ij})^{n_{ij}}\right]^{-1/2n_{ij}}, \quad (3)$$

$$\zeta_{ij} = \sum_{i\neq j\neq k}^{M} f_c(r_{ik})g(\theta_{jik})\exp[\gamma_{ij}^3(r_{ij} - r_{ik})^3], \quad (4)$$

$$g(\theta_{jik}) = 1 + \left(\frac{c_{ij}}{d_{ij}}\right)^2 - \frac{c_{ij}^2}{d_{ij}^2 + (h_{ij} - \cos\theta_{jik})^2}, \quad (5)$$

where f_c is the cutoff function, θ_{jik} is the angle between the line segment from atom i to atom j and the line segment from atom i to atom k, and the parameters A_{ij}, B_{ij}, etc are shown in tables 1 and 2. Units for each parameter are shown unless the parameter is dimensionless. These parameters were determined by Migliorato *et al* [3], who reused parameters from [15–17], but refitted the parameters for In–As bonds in order to better reproduce the cohesive energy of InAs. They

Table 1. Tersoff parameters for Ga–Ga, In–In, and As–As bonds.

Parameter	Ga–Ga	In–In	As–As
A_{ij} (eV)	993.888	2975.54	1571.86
B_{ij} (eV)	136.123	360.61	546.432
λ_{ij}	2.508 427 47	2.6159	2.38413
μ_{ij}	1.490 824	1.68117	1.728 73
c_{ij}	0.076 297 73	0.084 215	5.273 1318
d_{ij}	19.796 474	19.2626	0.751 026 62
h_{ij}	7.145 9174	7.392 28	0.152 923 54
β_{ij}	0.235 862 37	2.108 71	0.007 488 09
n_{ij}	3.472 9041	3.402 23	0.608 791 33
γ_{ij} (nm^{-1})	14.91	0.0	17.29
R_{ij} (nm)	0.35	0.35	0.35
D_{ij} (nm)	0.01	0.01	0.01

Table 2. Tersoff parameters for Ga–As, In–As, and Ga–In bonds.

Parameter	Ga–As	In–As	Ga–In
A_{ij} (eV)	2543.297	2291.292 969	1214.917
B_{ij} (eV)	314.46	424.874 512	177.22
λ_{ij}	2.828 093	2.517 917	2.5621
μ_{ij}	1.723 012	1.678 611	1.586 00
c_{ij}	1.226 302	0.9989	0.080 256
d_{ij}	0.790 396	0.826 08	195.2950
h_{ij}	−0.518 489	−0.5145	7.269 10
β_{ij}	0.357 192	0.3779	0.705 24
n_{ij}	6.317 410	7.141 472	3.437 39
γ_{ij} (nm^{-1})	17.23	15.0	0.0
R_{ij} (nm)	0.35	0.37	0.35
D_{ij} (nm)	0.01	0.01	0.01

fitted the parameters for InAs to its bulk modulus, $(c_{11} + 2c_{12})/3 = 57.9$ GPa, and its shear constant, $(c_{11} - c_{12})/2 = 19.0$ GPa. The empirical potential leads to a value for $c_{44} = 41.7$ MPa, which is slightly different from the experimental value 39.59 MPa [8].

The boundary conditions in the molecular statics simulations are periodic with a fixed volume. Since the QWR is assumed to be infinitely long along the y-direction and its strain state independent of y, the thickness of this unit cell along this direction is taken to be $8a$. Too small a value of the thickness would lead to an unphysical dependence of the strain on y. The size of the unit cell in its x and z dimensions is chosen to be large enough so that periodic images do not interact. A unit cell length and width in the xz-plane of $256a \times 256a$ was found to be sufficient. The total number of atoms used in this simulation is 4194 304. In the initial configuration of the simulation, the lattice constant of the InAs of the QWR is taken to be that of GaAs. Since the actual lattice constant of InAs is about 7% larger than this [8], this causes an initial compressive strain of about 7% in the wire. The system was relaxed from this initial configuration using the Polak–Ribière conjugate gradient algorithm as implemented in the software LAMMPS [18].

It should be noted that one can exploit the periodic boundary conditions to simulate an *array* of QWRs or QDs. However, if the unit cells of this array are of fixed volume, as is the case when applying the conjugate gradient algorithm in LAMMPS [19], then the displacement of the matrix at the boundary of the cell is fixed to zero, which is unphysical for

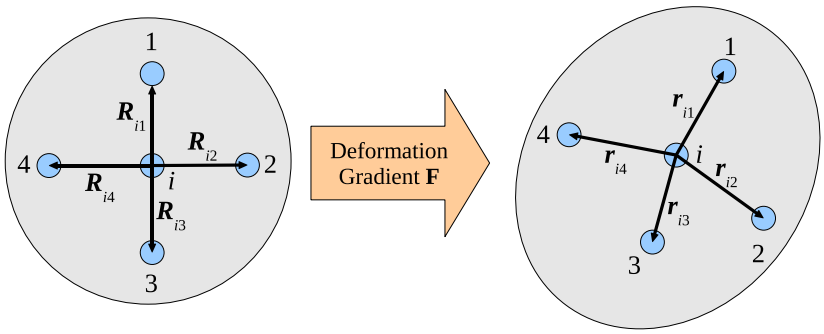

Figure 2. Relative positions of the neighbours of atom i before and after the deformation gradient $\mathbf{F}$ is applied.

closely spaced arrays. Because of this, only a isolated QWR is modelled in this work.

The strain is determined according to a least-squares formulation from [20] and simplified in [21]. The simplified formulation was also used in the atomistic visualization software AtomEye [22, 23]. For a given atom i with N neighbours within its cutoff radius, one can determine the vectors $\boldsymbol{R}_{i1}, \boldsymbol{R}_{i2}, \ldots, \boldsymbol{R}_{iN}$, which are the differences between the initial position vectors of the neighbours and the initial position vector of atom i. After a deformation gradient $\mathbf{F}$ is applied, these difference vectors become $\boldsymbol{r}_{i1}, \boldsymbol{r}_{i2}, \ldots, \boldsymbol{r}_{iN}$, the differences between the position vectors of the neighbours and the position vector of atom i after deformation. This is illustrated schematically in figure 2 for $N = 4$. For this work, the cutoff radius is the maximum value of $R_{ij} + D_{ij}$, which is 0.38 nm, as can be seen from tables 1 and 2. This will generally mean that the neighbours of the atom in each calculation of the strain will be the nearest ones.

According to the Cauchy–Born approximation [24],

$$\boldsymbol{r}_{ij} - \mathbf{F}\boldsymbol{R}_{ij} = \mathbf{0} \tag{6}$$

where $j \in 1, 2, \ldots, N$. Here, the Cauchy–Born approximation is not taken to be exact, but rather $\boldsymbol{r}_{ij} - \mathbf{F}\boldsymbol{R}_{ij}$ is treated as a residual to be minimized. From [20], the function to be minimized is

$$\boldsymbol{\phi}(\mathbf{F}) = \sum_{j=1}^{N} |\boldsymbol{r}_{ij} - \mathbf{F}\boldsymbol{R}_{ij}|^2 W(j) \tag{7}$$

where $W(j)$ is a weighting function. Following [21] and [22], (7) is simplified by taking $W(j)$ to be unity. With this simplification, the value of $\mathbf{F}$ that minimizes $\boldsymbol{\phi}$ is

$$\mathbf{F} = \mathbf{W}\mathbf{V}^{-1} \tag{8}$$

where

$$\mathbf{W} = \sum_{j=1}^{N} (\boldsymbol{r}_{ij} \otimes \boldsymbol{R}_{ij}) \tag{9}$$

$$\mathbf{V} = \sum_{j=1}^{N} (\boldsymbol{R}_{ij} \otimes \boldsymbol{R}_{ij}) \tag{10}$$

where $\otimes$ is the dyad product. From the deformation gradient $\mathbf{F}$, the gradient of the displacement $\nabla \boldsymbol{u}$ can be determined as

$$\nabla \boldsymbol{u} = \mathbf{F} - \mathbf{I} \tag{11}$$

where $\mathbf{I}$ is the identity tensor. From this, the small strain tensor [25] $\boldsymbol{\gamma}$ can be calculated as

$$\boldsymbol{\gamma} = \tfrac{1}{2}\left[\nabla \boldsymbol{u} + (\nabla \boldsymbol{u})^{\mathrm{T}}\right] \tag{12}$$

where the superscript T indicates the transpose. The small strain tensor is used here for the sake of consistency, since it is used in the linear elastic continuum methods of section 3.

3. Continuum methods

Indicial notation is used in this section, and unless otherwise stated, indices range from 1 to 3. The comma notation is used to indicate differentiation with respect to a coordinate. The values of the elastic constants of GaAs and InAs can be found in [8].

Suppose that out of an infinite space of GaAs, an infinitely long wire of GaAs with a square cross-section is cut out. The cutout is then transformed into InAs. Since the lattice constant of InAs is about 7% larger than that of GaAs, this has the effect of inducing a strain γ^*_{ij} where $\gamma^*_{ii} \approx 7\%$ (no sum on i) and all other components of the strain γ^*_{ij} are zero. No stress corresponds to this strain γ^*_{ij}, which is called the transformational strain or *eigenstrain*. To reinsert the transformed cutout, a strain of $-\gamma^*_{ij}$ is imposed to shrink the cutout to the original size it had before the transformation. This strain does correspond to a stress, namely $-C^{(\mathrm{w})}_{ijkl}\gamma^*_{kl}$, where $C^{(\mathrm{w})}_{ijkl}$ is the elasticity tensor of the QWR, that is, the InAs cutout. After reinsertion, the cutout is welded to the infinite space, so there is no slip between the InAs and GaAs, and the cutout is allowed to relax. The relaxation causes the InAs to expand, inducing a strain γ_{ij} in the surrounding GaAs matrix. A diagram of this result is shown in figure 3. The grid lines are distorted to show the strain in the GaAs and InAs. The stress in the matrix is $C^{(\mathrm{m})}_{ijkl}\gamma_{kl}$, where $C^{(\mathrm{m})}_{ijkl}$ is the elasticity tensor of the GaAs, the material of the matrix surrounding the QWR. The stress state from the initial strain, $\sigma^o_{ij} = -C^{(\mathrm{w})}_{ijkl}\gamma^*_{kl}$, is then superposed onto the so-called 'total' stress in the wire to

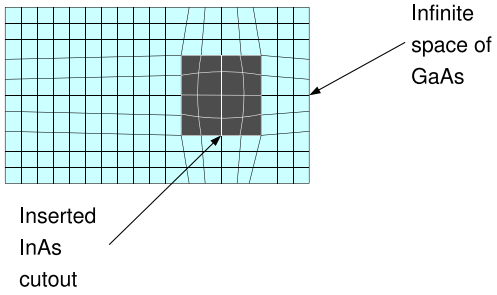

Figure 3. InAs cutout inserted back into space of GaAs. The grid lines illustrate the distortion of the reinserted InAs and the surrounding GaAs matrix.

account for the nonzero initial stress $\sigma_{ij}^{\mathrm{t}} = C_{ijkl}^{(\mathrm{w})}\gamma_{kl}$, so the real stress in the wire is [5, 26]

$$\sigma_{ij} = \sigma_{ij}^{\mathrm{t}} + \sigma_{ij}^{o} \tag{13}$$

$$= C_{ijkl}^{(\mathrm{w})}(\gamma_{kl} - \gamma_{kl}^{*}). \tag{14}$$

From here, both the boundary element and inclusion methods can be derived.

The exact value of the eigenstrain is actually slightly ambiguous. When the stress-free strain is applied to the cutout, then

$$\gamma_{11}^{*} = \frac{\partial u_1}{\partial x_1}. \tag{15}$$

Since the eigenstrain is constant, the above equation can be integrated such that

$$u_1 = \gamma_{11}^{*} x_1 \tag{16}$$

where the integration constant is set to zero because the displacement at the origin is taken to be zero. Let there be a cutout whose dimensions were originally $ka_{\mathrm{GaAs}} \times ka_{\mathrm{GaAs}}$ but are $ka_{\mathrm{InAs}} \times ka_{\mathrm{InAs}}$ after the stress-free strain is applied, where a_{GaAs} and a_{InAs} are the lattice constants of GaAs and InAs, respectively, and k is a positive integer. The lattice constant of GaAs, as noted before is 0.565 33 nm, while the lattice constant of InAs is 0.605 83 nm [8]. Let the displacement u_1 be determined for a point on the right boundary of the cutout. Then, u_1 is $k(a_{\mathrm{InAs}} - a_{\mathrm{GaAs}})$. Since in a small strain formulation, the distinction between the initial and deformed coordinates is treated as irrelevant [25], the value of x_1 on the right boundary can be taken as either ka_{GaAs} or ka_{InAs}, and γ_{11}^{*} can be taken to be either $(a_{\mathrm{InAs}} - a_{\mathrm{GaAs}})/a_{\mathrm{GaAs}}$ or $(a_{\mathrm{InAs}} - a_{\mathrm{GaAs}})/a_{\mathrm{InAs}}$. A similar argument applies for the other normal components of the eigenstrain. Depending on which way the eigenstrain is determined, one would have $\gamma_{ii}^{*} = 7.16\%$ or $\gamma_{ii}^{*} = 6.69\%$ (no sum on i). Paladugu *et al* [27] used the former value for the eigenstrain, while Guo *et al* [28] used the latter.

3.1. Boundary element method

If there is an initial stress σ_{ij}^{o}, then the Somigliana's identity is modified to become [29]

$$cu_l = \int_\Gamma U_{lk} t_k \,\mathrm{d}\Gamma - \int_\Gamma T_{lk} u_k \,\mathrm{d}\Gamma - \int_\Omega \sigma_{jk}^{o} U_{lk,j} \,\mathrm{d}\Omega \tag{17}$$

where Γ is the boundary of the QWR. When dealing with points inside the QWR, Ω is the space inside the QWR. When dealing with points outside the QWR, Ω would be the space outside the QWR, that is, the GaAs matrix, but in this space, σ_{jk}^{o} is zero. On the right-hand side of (17), u_k and t_k are the displacement and traction along Γ. On the left-hand side of (17), u_l is the displacement at some particular point. If this point is a smooth boundary point, then $c = 1/2$, and if it is within Ω but not on the boundary, then $c = 1$. U_{lk} and T_{lk} are the Green's functions of displacement and traction in the k-direction due to a unit load in the l-direction. The last integral is a domain integral, but since the eigenstrain γ_{ij}^{*} is constant, it can be transformed into a boundary integral as follows.

$$\int_\Omega \sigma_{jk}^{o} U_{lk,j} \,\mathrm{d}\Omega = \int_\Omega (\sigma_{jk}^{o} U_{lk})_{,j} \,\mathrm{d}\Omega = \int_\Gamma \sigma_{jk}^{o} U_{lk} n_j \,\mathrm{d}\Gamma \tag{18}$$

$$= -\int_\Gamma C_{jkmn}\gamma_{mn}^{*} U_{lk} n_j \,\mathrm{d}\Gamma \tag{19}$$

where n_j is the outward unit normal to the boundary Γ. Equation (17) can then be simplified to

$$cu_l = \int_\Gamma U_{lk}(t_k + C_{jkmn}\gamma_{mn}^{*} n_j) \,\mathrm{d}\Gamma - \int_\Gamma T_{lk} u_k \,\mathrm{d}\Gamma. \tag{20}$$

In [5], building from the work in [30], U_{lk} is expressed in the Stroh formalism.

$$U_{ij} = \frac{1}{\pi}\mathrm{Im}\,[A_{jm} D_{mn} A_{in}] \tag{21}$$

where $\mathrm{Im}\,(Z)$ is the imaginary part of the complex number Z, and

$$D_{mn} = \begin{cases} \ln(z_m - s_m) & m = n \\ 0 & m \neq n \end{cases} \tag{22}$$

where

$$z_j = x + p_j z \tag{23}$$

$$s_j = X + p_j Z. \tag{24}$$

The ordered pairs (x, z) and (X, Z) are the coordinates of the field and source points in the 1–3 plane (or xz-plane), p_j is a Stroh eigenvalue, and A_{jr} is the jrth component of the matrix of Stroh eigenvectors $\mathbf{A} = [\boldsymbol{a}_1\, \boldsymbol{a}_2\, \boldsymbol{a}_3]$. p_j and $\boldsymbol{a}_j$ must satisfy the eigenequation

$$[\mathbf{Q} + p_j(\mathbf{R} + \mathbf{R}^{\mathrm{T}}) + p_j^2 \mathbf{T}]\boldsymbol{a}_j = 0 \tag{25}$$

where

$$Q_{ik} = C_{i1k1} \qquad R_{ik} = C_{1ik3} \qquad T_{ik} = C_{i3k3}. \tag{26}$$

The superscript T indicates the transpose, and C_{ijkl} is the elasticity tensor. There are six eigenvalues, but j ranges from 1 to 3, and $p_{j+3} = \bar{p}_j$, where the overbar indicates the complex conjugate. The first three eigenvalues are chosen such that

$$\mathrm{Im}\,(p_j) > 0 \qquad \boldsymbol{a}_{j+3} = \bar{\boldsymbol{a}}_j \qquad \boldsymbol{b}_{j+3} = \bar{\boldsymbol{b}}_j \tag{27}$$

where

$$\boldsymbol{b}_j = (\mathbf{R} + p_j \mathbf{T})\boldsymbol{a}_j = \frac{1}{p_j}(\mathbf{Q} + p_j \mathbf{R})\boldsymbol{a}_j \quad (\text{no sum on } j). \tag{28}$$

The eigenvectors are normalized such that they satisfy the relation

$$\boldsymbol{b}_i^{\mathrm{T}}\boldsymbol{a}_j + \boldsymbol{a}_i^{\mathrm{T}}\boldsymbol{b}_j = \delta_{ij} \tag{29}$$

where

$$\delta_{ij} = \begin{cases} 1 & i = j \\ 0 & i \neq j. \end{cases} \tag{30}$$

The traction Green's function can be derived from the displacement Green's function [5]. Barring the presence of eigenstrain, which is taken into account by the last term on the right-hand side of (17), not by the Green's functions themselves, the elastic strain is

$$\gamma_{jk} = \tfrac{1}{2}(u_{j,k} + u_{k,j}). \tag{31}$$

Similarly, then, the strain Green's function is

$$\gamma^i_{jk} = \tfrac{1}{2}(U_{ij,k} + U_{ik,j}). \tag{32}$$

The traction is

$$t_j = C_{jklm}\gamma_{lm}n_k \tag{33}$$

where n_k is the kth component of the outward normal. Therefore, the traction Green's function is

$$T_{ij} = C_{jklm}\gamma^i_{lm}n_k = \tfrac{1}{2}C_{jklm}n_k(U_{il,m} + U_{im,l}). \tag{34}$$

Substituting (21) into (34),

$$T_{ij} = \frac{C_{jklm}n_k}{2\pi}\mathrm{Im}\left[A_{ln}D_{nr,m}A_{ir} + A_{mn}D_{nr,l}A_{ir}\right]. \tag{35}$$

Now

$$D_{nr,m} = \begin{cases} z_{n,m}/(z_n - s_n) & n = r \\ 0 & n \neq r \end{cases} \quad (\text{no sum on } n) \tag{36}$$

since $s_{n,m} = 0$, where the derivative is with respect to the point (x, z). Furthermore,

$$z_{n,1} = \frac{\partial z_n}{\partial x} = 1 \tag{37}$$

$$z_{n,2} = \frac{\partial z_n}{\partial y} = 0 \tag{38}$$

$$z_{n,3} = \frac{\partial z_n}{\partial z} = p_n. \tag{39}$$

From the above, the traction Green's function T_{ij} can be readily determined.

Approximating the boundary with M constant elements, the discretization of (20) is then

$$cu_l = \sum_{i=1}^{M}\left(\int_{\Gamma_i} U^{(\mathrm{m})}_{lk}\,\mathrm{d}\Gamma_i\right)t^{(\mathrm{m})}_{ki} - \sum_{i=1}^{M}\left(\int_{\Gamma_i} T^{(\mathrm{m})}_{lk}\,\mathrm{d}\Gamma_i\right)u_{ki} \tag{40}$$

for the GaAs matrix, and

$$cu_l = \sum_{i=1}^{M}\left(\int_{\Gamma_i} U^{(\mathrm{w})}_{lk}\,\mathrm{d}\Gamma_i\right)(t^{(\mathrm{w})}_{ki} + C^{(\mathrm{w})}_{rkmn}\gamma^*_{mn}n_r) - \sum_{i=1}^{M}\left(\int_{\Gamma_i} T^{(\mathrm{w})}_{lk}\,\mathrm{d}\Gamma_i\right)u_{ki} \tag{41}$$

for the InAs wire. Superscripts in parentheses are not indices and are not summed. In (40) and (41), M is the number of elements and also the number of nodes, Γ_i is the portion of the boundary discretized by the ith element, u_{ki} is the component of the displacement in the k-direction for the ith node, which is at the shared boundary of the GaAs matrix and the InAs wire, and $t^{(\mathrm{m})}_{ki}$ is the component of the traction at the boundary of the GaAs matrix in the k-direction for the ith node. This traction is with respect to the outer normal of the matrix boundary, which points away from the GaAs matrix and toward the InAs wire. Similarly, the term $t^{(\mathrm{w})}_{ki}$ is the component of the traction at the boundary of the InAs wire in the k-direction for the ith node. This traction is with respect to the outer normal of the wire boundary, which points toward the GaAs matrix and away from the InAs wire. Accordingly, $t^{(\mathrm{m})}_{ki} = -t^{(\mathrm{w})}_{ki}$. $U^{(\mathrm{m})}_{lk}$ and $T^{(\mathrm{m})}_{lk}$ are the Green's functions for the GaAs matrix. They have the same form as (21), but with elastic stiffness $C_{jkmn} = C^{(\mathrm{m})}_{jkmn}$. Similarly, $U^{(\mathrm{w})}_{lk}$ and $T^{(\mathrm{w})}_{lk}$ are the Green's functions for the InAs wire.

The above discretized integral equations can be rewritten in matrix form. Let

$$[\hat{U}^{(\mathrm{m})}_{lk}]_{ji} \equiv \left.\int_{\Gamma_i} U^{(\mathrm{m})}_{lk}\,\mathrm{d}\Gamma_i\right|_j \tag{42}$$

$$[\hat{U}^{(\mathrm{w})}_{lk}]_{ji} \equiv \left.\int_{\Gamma_i} U^{(\mathrm{w})}_{lk}\,\mathrm{d}\Gamma_i\right|_j \tag{43}$$

$$[\hat{T}^{(\mathrm{m})}_{lk}]_{ji} \equiv \left.\left(\int_{\Gamma_i} T^{(\mathrm{m})}_{lk}\,\mathrm{d}\Gamma_i + \tfrac{1}{2}\delta_{lk}\delta_{ji}\right)\right|_j \tag{44}$$

$$[\hat{T}^{(\mathrm{w})}_{lk}]_{ji} \equiv \left.\left(\int_{\Gamma_i} T^{(\mathrm{w})}_{lk}\,\mathrm{d}\Gamma_i + \tfrac{1}{2}\delta_{lk}\delta_{ji}\right)\right|_j \tag{45}$$

$$[\hat{F}_l]_j \equiv \left.\sum_{i=1}^{M}\left(\int_{\Gamma_i} U^{(\mathrm{m})}_{lk}\,\mathrm{d}\Gamma_i\right)C^{(\mathrm{w})}_{rkmn}\gamma^*_{mn}n_r\right|_j \tag{46}$$

$$[u_k]_i \equiv u_{ki} \tag{47}$$

$$[t^{(\mathrm{m})}_k]_i \equiv t^{(\mathrm{m})}_{ki} \tag{48}$$

$$[t^{(\mathrm{w})}_k]_i \equiv t^{(\mathrm{w})}_{ki}. \tag{49}$$

The notation $f|_j$ means to evaluate f at the jth node. Rewriting (40) and (41) (for $i = 1, 2, \ldots, M$),

$$\sum_{i=1}^{M}[\hat{T}^{(\mathrm{m})}_{lk}]_{ji}[u_k]_i - \sum_{i=1}^{M}[\hat{U}^{(\mathrm{m})}_{lk}]_{ji}[t^{(\mathrm{m})}_k]_i = 0 \tag{50}$$

$$\sum_{i=1}^{M}[\hat{T}^{(\mathrm{w})}_{lk}]_{ji}[u_k]_i - \sum_{i=1}^{M}[\hat{U}^{(\mathrm{w})}_{lk}]_{ji}[t^{(\mathrm{w})}_k]_i = [\hat{F}_l]_j. \tag{51}$$

Since $t^{(\mathrm{m})}_{ki} = -t^{(\mathrm{w})}_{ki}$, the above equations can be combined into a single matrix equation, shown below, where *both* the displacements and the tractions on the boundary of the wire appear as unknowns.

$$\begin{bmatrix} \hat{\mathbf{T}}^{(\mathrm{m})} & \hat{\mathbf{U}}^{(\mathrm{m})} \\ \hat{\mathbf{T}}^{(\mathrm{w})} & -\hat{\mathbf{U}}^{(\mathrm{w})} \end{bmatrix}\begin{bmatrix} \mathbf{u} \\ \mathbf{t}^{(\mathrm{w})} \end{bmatrix} = \begin{bmatrix} \mathbf{0} \\ \mathbf{F} \end{bmatrix}. \tag{52}$$

Here, $[\hat{U}_{lk}^{(\mathrm{m})}]_{ji}$ is the jith 3×3 submatrix of the $3M \times 3M$ matrix $\hat{\mathbf{U}}^{(\mathrm{m})}$, and similarly for $\hat{\mathbf{T}}^{(\mathrm{m})}$, $\hat{\mathbf{U}}^{(\mathrm{w})}$, and $\hat{\mathbf{T}}^{(\mathrm{w})}$. Likewise, $[u_k]_i$ represents the ith 3×1 submatrix of the $3M \times 1$ matrix $\mathbf{u}$, $[t_k^{(\mathrm{m})}]_i$ and $[t_k^{(\mathrm{w})}]_i$ are the ith 3×1 submatrices of $\mathbf{t}^{(\mathrm{m})}$ and $\mathbf{t}^{(\mathrm{w})}$, respectively, and $[\hat{F}_l]_j$ is the jth 3×1 submatrix of $\mathbf{F}$. The matrix $\mathbf{0}$ is the $3M \times 1$ zero vector.

The integrals in (40) and (41) can be evaluated exactly [5]. In general, one can write

$$\int_{\Gamma_s} U_{ij}\,\mathrm{d}\Gamma_s = \frac{1}{\pi}\mathrm{Im}\left[A_{jm}H_{mn}^{\Gamma_s}A_{in}\right] \tag{53}$$

$$\int_{\Gamma_s} T_{ij}\,\mathrm{d}\Gamma_s = \frac{C_{jklm}n_k}{2\pi}\mathrm{Im}\left[A_{ln}\hat{H}_{nrm}^{\Gamma_s}A_{ir} + A_{mn}\hat{H}_{nrl}^{\Gamma_s}A_{ir}\right] \tag{54}$$

where $H_{mn}^{\Gamma_i} \equiv \int_{\Gamma_i} D_{mn}\,\mathrm{d}\Gamma_i$ and $\hat{H}_{nrm}^{\Gamma_i} \equiv \int_{\Gamma_i} D_{nr,m}\,\mathrm{d}\Gamma_i$. However, (54) is not used to evaluate the submatrices $[\hat{T}_{lk}^{(\mathrm{m})}]_{ji}$ and $[\hat{T}_{lk}^{(\mathrm{w})}]_{ji}$ if they are along the diagonal of $\hat{\mathbf{T}}^{(\mathrm{m})}$ and $\hat{\mathbf{T}}^{(\mathrm{w})}$, respectively. This will be discussed at the end of this section. Now

$$H_{mn}^{\Gamma_i} = \int_{\Gamma_i} D_{mn}\,\mathrm{d}\Gamma_i = \int_{\tau_1}^{\tau_2} D_{mn}\frac{\partial\Gamma_i}{\partial\tau}\,\mathrm{d}\tau \tag{55}$$

$$\hat{H}_{nrm}^{\Gamma_i} = \int_{\Gamma_i} D_{nr,m}\,\mathrm{d}\Gamma_i = \int_{\tau_1}^{\tau_2} D_{nr,m}\frac{\partial\Gamma_i}{\partial\tau}\,\mathrm{d}\tau. \tag{56}$$

Since constant elements are used, Γ_i is a line segment connecting the endpoints of the ith constant element, which are here denoted as (x_1^i, z_1^i) and (x_2^i, z_2^i). The line segment Γ_i may be expressed as the set of coordinates (x^i, z^i) that satisfy the relations

$$x^i = x_1^i + (x_2^i - x_1^i)\tau \tag{57}$$

$$z^i = z_1^i + (z_2^i - z_1^i)\tau \tag{58}$$

where $0 \leqslant \tau \leqslant 1$. For these relations, τ_1 and τ_2 in (55) and (56) equal zero and one, respectively, and $\partial\Gamma_i/\partial\tau = l$, where l is the length of the line segment Γ_i. Accordingly,

$$H_{mn}^{\Gamma_i} = \int_0^1 D_{mn} l\,\mathrm{d}\tau = \begin{cases} h_m l & m = n \\ 0 & m \neq n \end{cases} \tag{59}$$

where

$$h_m = \frac{x_1^i + p_m z_1^i - s_m}{x_2^i - x_1^i + p_m(z_2^i - z_1^i)}\ln\left(\frac{x_2^i + p_m z_2^i - s_m}{x_1^i + p_m z_1^i - s_m}\right) + \ln(x_2^i + p_m z_2^i - s_m) - 1 \quad (\text{no sum on } i \text{ or } m) \tag{60}$$

and

$$\hat{H}_{nrm}^{\Gamma_i} = \int_0^1 D_{nr,m} l\,\mathrm{d}\tau = \begin{cases} \hat{h}_{nm} l & n = r \\ 0 & n \neq r \end{cases} \tag{61}$$

where

$$\hat{h}_{nm} = \frac{z_{n,m}}{x_2^i - x_1^i + p_n(z_2^i - z_1^i)}\ln\left(\frac{x_2^i + p_n z_2^i - s_n}{x_1^i + p_n z_1^i - s_n}\right) \quad (\text{no sum on } n). \tag{62}$$

The values of $z_{n,m}$ for $m = 1, 2, 3$ are shown in (37)–(39) above.

Equation (54) is only used to evaluate $\int_{\Gamma_i} T_{lk}\,\mathrm{d}\Gamma_i|_j$ if $i \neq j$. Otherwise, the rigid body method [29] is used. For the infinite domain of the GaAs matrix,

$$[\hat{T}_{lk}^{(\mathrm{m})}]_{jj} = \delta_{lk} - \sum_{i\neq j}^{M}[\hat{T}_{lk}^{(\mathrm{m})}]_{ji}. \tag{63}$$

For the finite domain of the InAs wire,

$$[\hat{T}_{lk}^{(\mathrm{w})}]_{jj} = -\sum_{i\neq j}^{M}[\hat{T}_{lk}^{(\mathrm{w})}]_{ji}. \tag{64}$$

Once u_{ki} and $t_{ki}^{(\mathrm{w})}$ (which is $-t_{ki}^{(\mathrm{m})}$) are determined, (40) can be used to find the displacement at an arbitrary point in the GaAs matrix, and (41) can be used to find the displacement at an arbitrary point in the InAs wire. Equation (40) or (41) may be substituted into (31) to find the strain at an internal point, and from the strain, the stress may be calculated.

The strains are determined for field points within the domain $x \in (-128a_{\mathrm{GaAs}}, 128a_{\mathrm{GaAs}})$, $z \in (-128a_{\mathrm{GaAs}}, 128a_{\mathrm{GaAs}})$ on a 500×500 grid evenly spaced over the whole domain, except for points deemed too close to the boundary of the QWR for this BEM to yield accurate strain values. Here, points within a distance δ, where δ is taken to be half the length of each boundary element, were taken to be too close. The boundary between the QWR and its surrounding matrix is discretized into 640 elements.

3.2. Inclusion method

If the difference in material properties between the QWR and its surrounding matrix is ignored, then the displacement at field point $\boldsymbol{X}$ can be written as [31]

$$u_l(\boldsymbol{X}) = -\int_\Omega \sigma_{jk}^o U_{lk,j}(\boldsymbol{X})\,\mathrm{d}\Omega \tag{65}$$

where the domain Ω is taken to be all space. Since the difference in material properties between the GaAs matrix and the InAs QWR is neglected, the function $U_{lk,j}$ is the same for all space, and the elasticity tensor is denoted as C_{ijkl}. The elastic properties of the QWR are taken to be those of the matrix. The domain Ω can be divided into two subdomains, $\Omega^{(\mathrm{m})}$ and $\Omega^{(\mathrm{w})}$, consisting of the points inside the matrix and the wire, respectively. Since $\sigma_{jk}^o = -C_{jkmn}\gamma_{mn}^*$, and γ_{mn}^* is only nonzero within $\Omega^{(\mathrm{w})}$, (65) becomes

$$u_l = \int_{\Omega^{(\mathrm{w})}} C_{jkmn}\gamma_{mn}^* U_{lk,j}\,\mathrm{d}\Omega \tag{66}$$

which can be rewritten as a boundary integral since $C_{jkmn}\gamma_{mn}^*$ is constant.

$$u_l = C_{jkmn}\gamma_{mn}^*\int_{\Omega^{(\mathrm{w})}} U_{lk,j}\,\mathrm{d}\Omega = C_{jkmn}\gamma_{mn}^*\int_\Gamma U_{lk}n_j\,\mathrm{d}\Gamma \tag{67}$$

where Γ is the boundary of the QWR and n_j is the outward pointing normal of this boundary. If the boundary is a series of straight line segments Γ_i, then (67) can be integrated

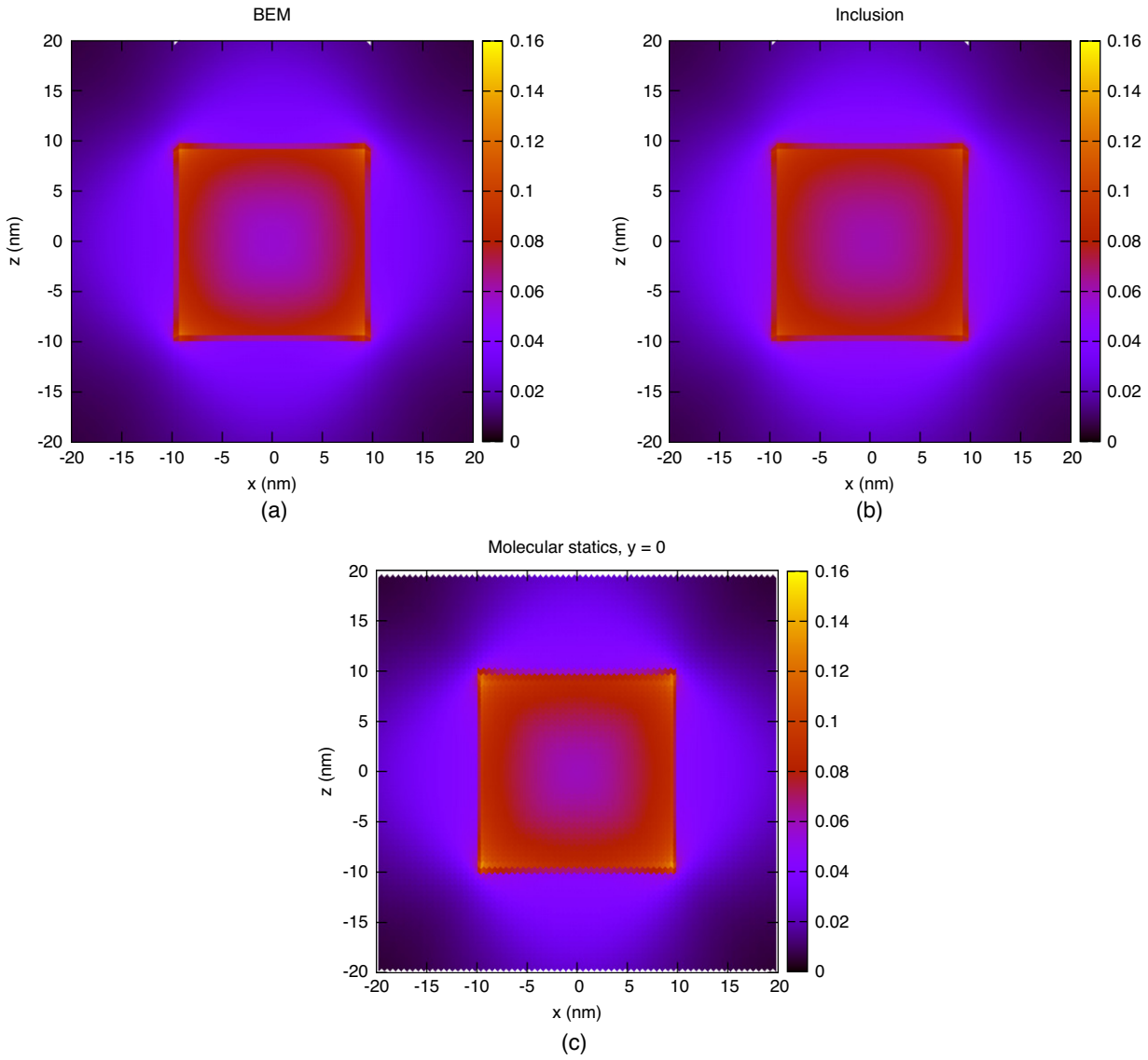

Figure 4. Maximum principal strains as determined by (a) BEM (for $\gamma_{ii}^{*} = 7.16\%$, no sum on i), (b) inclusion method (also for $\gamma_{ii}^{*} = 7.16\%$, no sum on i), and (c) molecular statics for atoms with initial y-coordinate equal to zero. $x, z \in [-20\text{ nm}, 20\text{ nm}]$. The y-axis points into the plane of the page.

analytically, and the contribution to the displacement from each line segment Γ_i is [6]

$$u_l = \frac{n_j C_{jkmn} \gamma_{mn}^{*}}{\pi} \mathrm{Im}\left[A_{kr} H_{rs}^{\Gamma_i} A_{ls}\right] \tag{68}$$

where A_{ij} is the ijth component of the matrix of Stroh eigenvectors discussed in section 3.1, and $H_{jk}^{\Gamma_i}$ is the same as in (59) from the same section. The total displacement is the sum of the contributions to the displacement from each line segment.

The above equation can be differentiated to obtain the strain.

$$\gamma_{\beta\alpha} = \frac{n_j C_{jkmn} \gamma_{mn}^{*}}{\pi} \mathrm{Im}\left[A_{kr} \hat{H}_{rs\alpha}^{\Gamma_i} A_{\beta s} + A_{kr} \hat{H}_{rs\beta}^{\Gamma_i} A_{\alpha s}\right] \tag{69}$$

$$\gamma_{2\alpha} = \frac{n_j C_{jkmn} \gamma_{mn}^{*}}{\pi} \mathrm{Im}\left[A_{kr} \hat{H}_{rs\alpha}^{\Gamma_i} A_{2s}\right] \tag{70}$$

where $\alpha, \beta = 1, 3$ and $\hat{H}_{jkl}^{\Gamma_i}$ is the same as in (61).

The strains were determined at the same field points used for the BEM, described above.

4. Results

Numerical computations are carried out on a PC with dual quad-core xeon 3.20 GHz processors and 4 GB of RAM. The molecular statics calculations with LAMMPS took approximately five days to complete. By contrast, on the same PC, a Fortran program implementing the BEM took about an hour to run its calculations, and a Fortran program implementing the inclusion method less than a minute. The molecular statics calculations ran in parallel using MPI and used all eight processor cores, while the Fortran programs for the continuum calculations ran in serial.

Figures 4 and 5 show colour (grayscale) maps of the maximum and minimum principal strains calculated by BEM, the inclusion method, and molecular statics. Noteworthy is

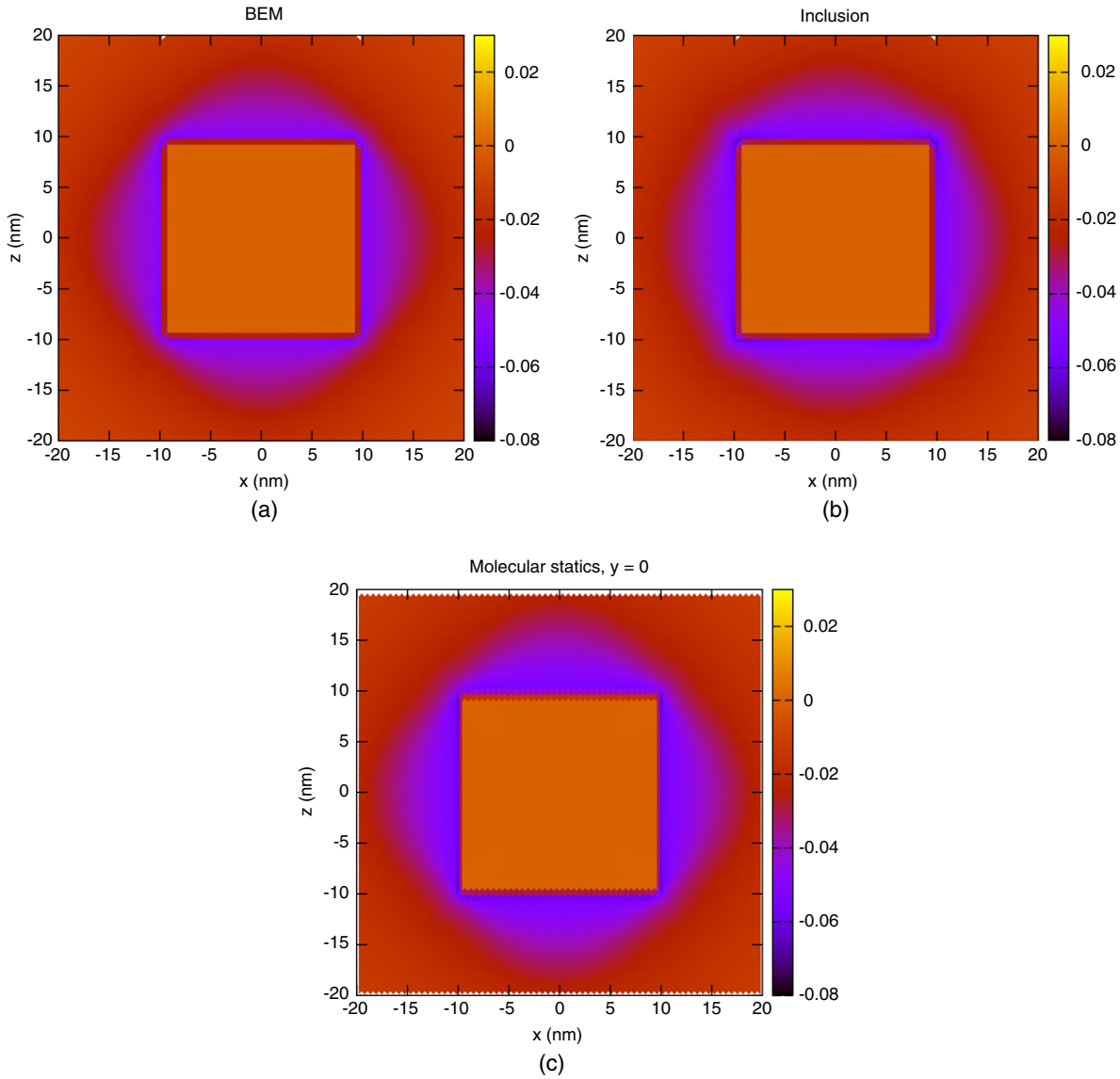

Figure 5. Minimum principal strains as determined by (a) BEM (for $\gamma_{ii}^* = 7.16\%$, no sum on i), (b) inclusion method (also for $\gamma_{ii}^* = 7.16\%$, no sum on i), and (c) molecular statics for atoms with y-coordinate equal to zero. $x, z \in [-20\text{ nm}, 20\text{ nm}]$. Again, the y-axis points into the plane of the page.

Table 3. Maximum principal strains at the centre of the QWR. γ_{ii}^* is a normal component of the eigenstrain, with no sum on i.

Method	Max. prin. strain
BEM, $\gamma_{ii}^* = 7.16\%$	0.056
BEM, $\gamma_{ii}^* = 6.69\%$	0.052
Inclusion, $\gamma_{ii}^* = 7.16\%$	0.061
Inclusion, $\gamma_{ii}^* = 6.69\%$	0.057
Molecular statics ($y = 0$)	0.059

Table 4. Minimum principal strains at $x = z = \pm 20$ nm. γ_{ii}^* is a normal component of the eigenstrain, with no sum on i.

Method	Min. prin. strain, $x = \pm 20$ rm
BEM, $\gamma_{ii}^* = 7.16\%$	−0.0098
BEM, $\gamma_{ii}^* = 6.69\%$	−0.0089
Inclusion, $\gamma_{ii}^* = 7.16\%$	−0.0103
Inclusion, $\gamma_{ii}^* = 6.69\%$	−0.0096
Molecular statics ($y = 0$)	−0.0113

that the map of the maximum principal strain for the inclusion method more closely resembles the maps for molecular statics than the map for the BEM. The principal strain fields as determined by molecular statics do not differ significantly as the y-coordinate changes—which makes sense since the QWR is under plane strain—so only the strains for the case where $y = 0$ are shown.

Figures 6 and 7 show profile plots of the maximum principal strain along the diagonal $x = z$ as determined using the BEM, inclusion method, and molecular statics. As can be observed, all methods predict approximately the same shape for the strain profile, and particularly outside the QWR, the

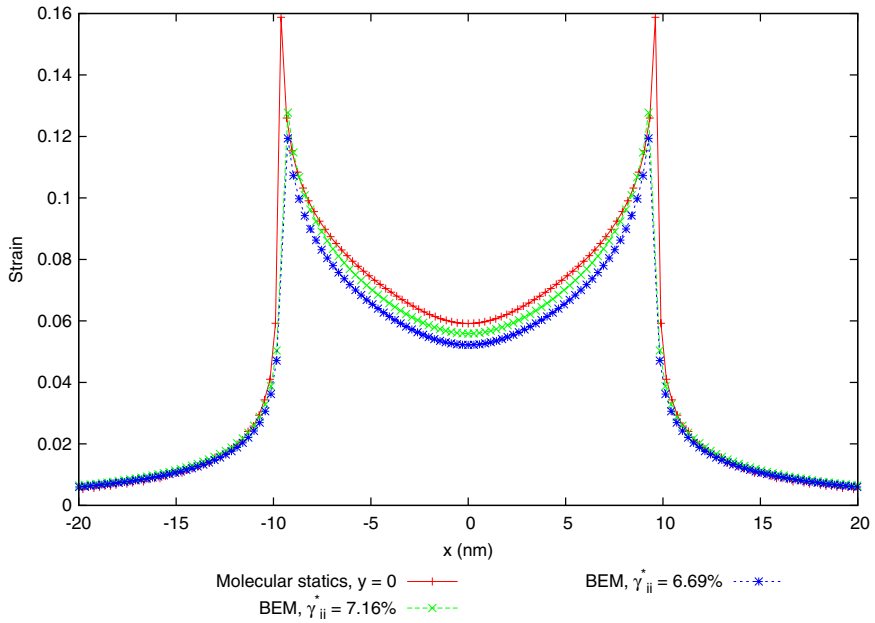

Figure 6. Maximum principal strain for points along the diagonal line $x = z$, for $x \in [-20\text{ nm}, 20\text{ nm}]$, using the BEM and molecular statics. γ^*_{ii} is a normal component of the eigenstrain, with no sum on i.

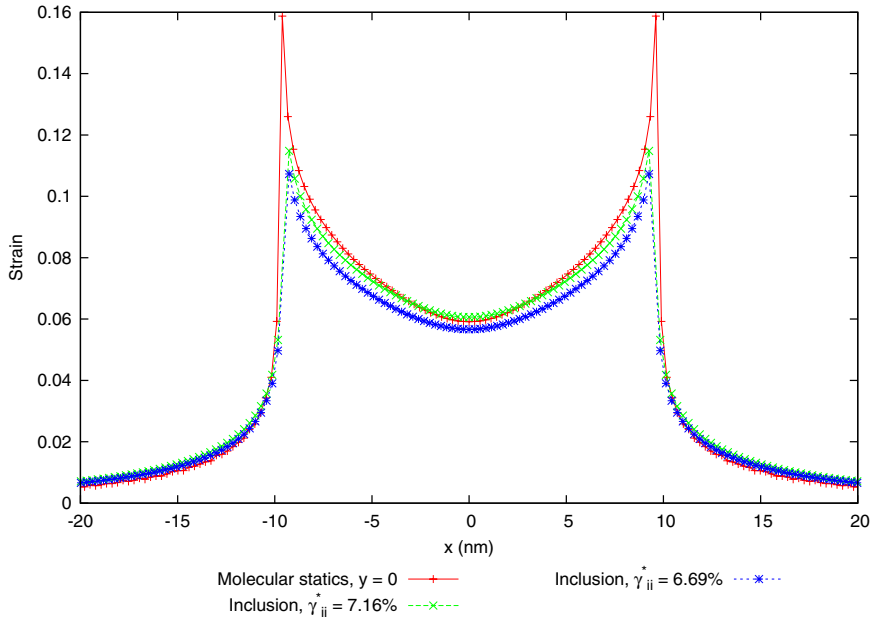

Figure 7. Maximum principal strain for points along the diagonal line $x = z$, for $x \in [-20\text{ nm}, 20\text{ nm}]$, using the inclusion method and molecular statics. γ^*_{ii} is a normal component of the eigenstrain, with no sum on i.

strain profiles are especially close to one another. Table 3 lists the values for the maximum principal strain at the centre of the QWR for these methods. The value from BEM differs from the value from molecular statics by either 5.1% or 11.9%, depending on how the eigenstrain is determined. (See section 3 on the ambiguity in determining eigenstrain.) Similarly, the value from the inclusion method differs from molecular statics by either −3.4% or 3.4%. Again, the results from the inclusion method are closer than the BEM results are to the results from molecular statics. Furthermore, the values from table 3 can be used to show that the induced maximum principal strain based on the continuum methods is linearly proportional to the eigenstrain. For example, the ratio of the eigenstrain to the maximum principal strain as determined from the BEM is $0.0716/0.056 \approx 0.0669/0.052 \approx 1.3$. This is consistent with the formulations presented in the previous section.

Similarly, figures 8 and 9 show profile plots of the minimum principal strain along the $x = z$ diagonal as determined using the BEM, inclusion method, and molecular statics. Again, the results from the inclusion method are closer than the BEM results are to the results from molecular statics. All three methods predict that the minimum principal strain

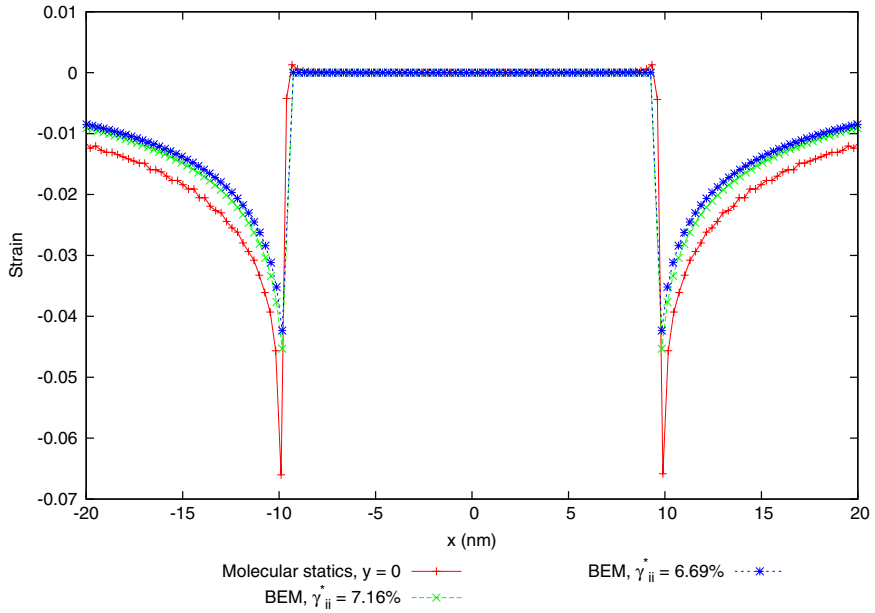

Figure 8. Minimum principal strain for points along the diagonal line $x = z$, for $x \in [-20\text{ nm}, 20\text{ nm}]$, using the BEM and molecular statics. γ^*_{ii} is a normal component of the eigenstrain, with no sum on i.

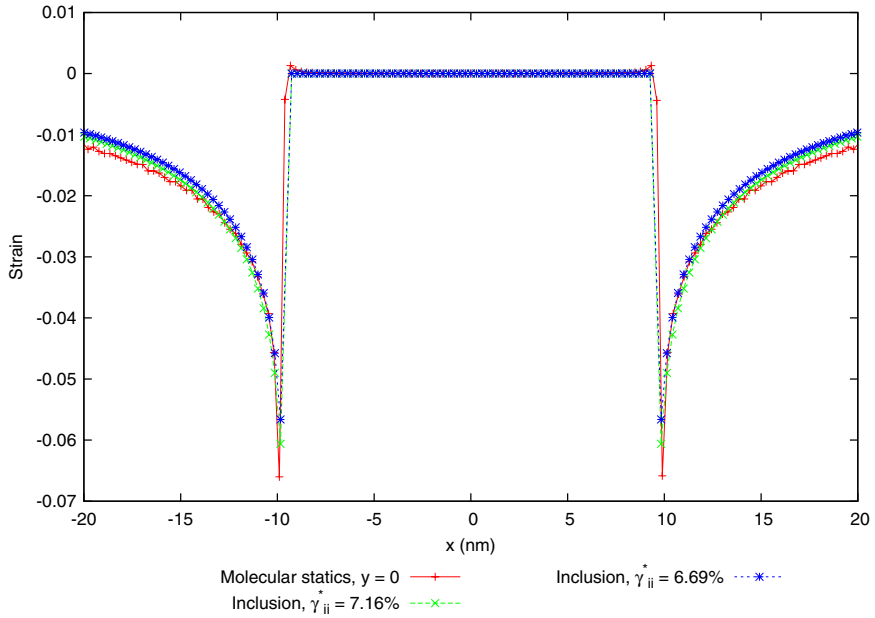

Figure 9. Minimum principal strain for points along the diagonal line $x = z$, for $x \in [-20\text{ nm}, 20\text{ nm}]$, using the inclusion method and molecular statics. γ^*_{ii} is a normal component of the eigenstrain, with no sum on i.

inside the QWR is zero. However, outside the QWR, the strain profiles show some disagreement. This is shown in table 4, where the minimum principal strains are given for the arbitrary points where $x = z = \pm 20$ nm.

Profiles of the gradients of the strain tensor, $\epsilon_{11,3}$, $\epsilon_{33,3}$, and $\epsilon_{13,3}$, along the diagonal $x = z$ are shown in figures 10–12. To simplify the figures, only the results for molecular statics for $y = 0$ and the continuum methods with $\gamma^*_{ii} = 7.16\%$ (no sum on i) are shown. These were determined numerically using central difference formulae. Because of the symmetry of the square QWR, these derivatives have the same values as $\epsilon_{33,1}$, $\epsilon_{11,1}$, and $\epsilon_{31,1}$, respectively. For each of the three approaches—molecular statics, BEM, and the inclusion method—the values of $\epsilon_{11,3}$, $\epsilon_{33,3}$, and $\epsilon_{13,3}$ are largely in agreement.

5. Discussion and conclusions

Although the inclusion method, unlike the BEM, ignores the difference in material properties between the QWR and its surrounding matrix, its results are in better agreement with the molecular statics results than the results from the BEM.

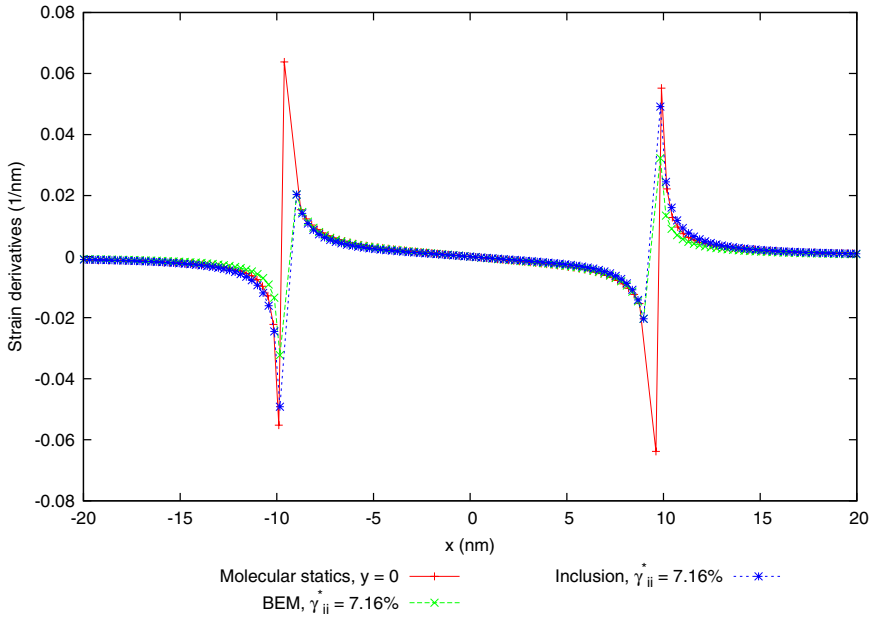

Figure 10. Strain derivative $\epsilon_{11,3}$ for points along the diagonal line $x = z$.

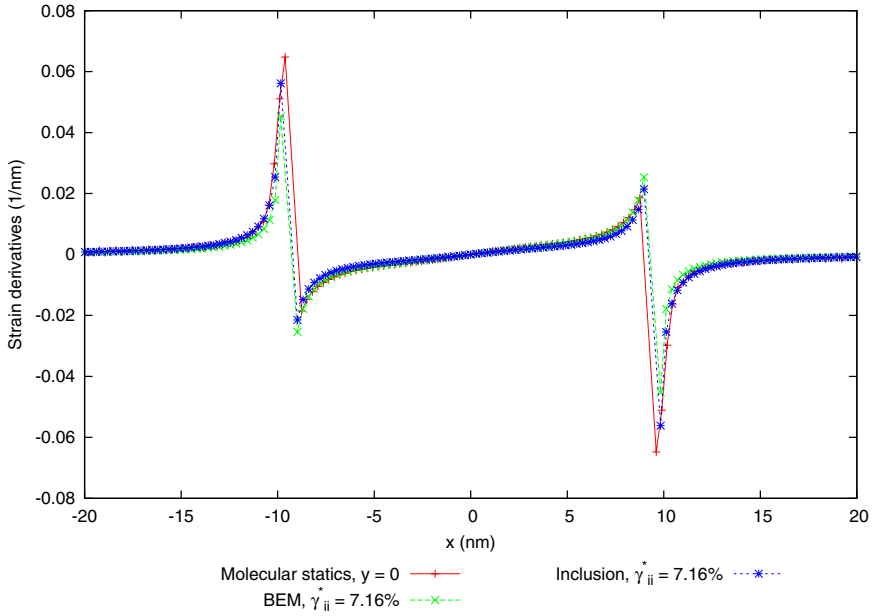

Figure 11. Strain derivative $\epsilon_{33,3}$ for points along the diagonal line $x = z$.

Faux *et al* [32] argued that since the elastic constants of III–V semiconductors are largely dependent on their lattice spacing [33], then the strain in the QWR induced by the lattice mismatch causes its effective elastic constants to be roughly those of its surrounding matrix. The results tentatively indicate that this argument may have some merit, although Ellaway and Faux [34] have pointed out that simply using the elastic constants of the matrix for the QWR is still a crude approximation at best. We remark that in future work, we plan to study further the dependence of the elastic constants on strain.

The maximum and minimum principal strains inside and around a QWR were determined by the following methods:

- the boundary element method (see section 3.1) and the inclusion method (see section 3.2), both of which are grounded in continuum mechanics and linear elasticity;
- molecular statics (see section 2), an atomistic approach suitable for the length scales of QWRs.

Based on the results from these methods, one can conclude that if one needs to predict the strain fields within the QWR to an accuracy of about 10%, then the continuum methods are adequate. Continuum methods are also capable of determining the qualitative trends in how strain fields vary. Furthermore, both continuum methods are far more computationally inexpensive than molecular statics.

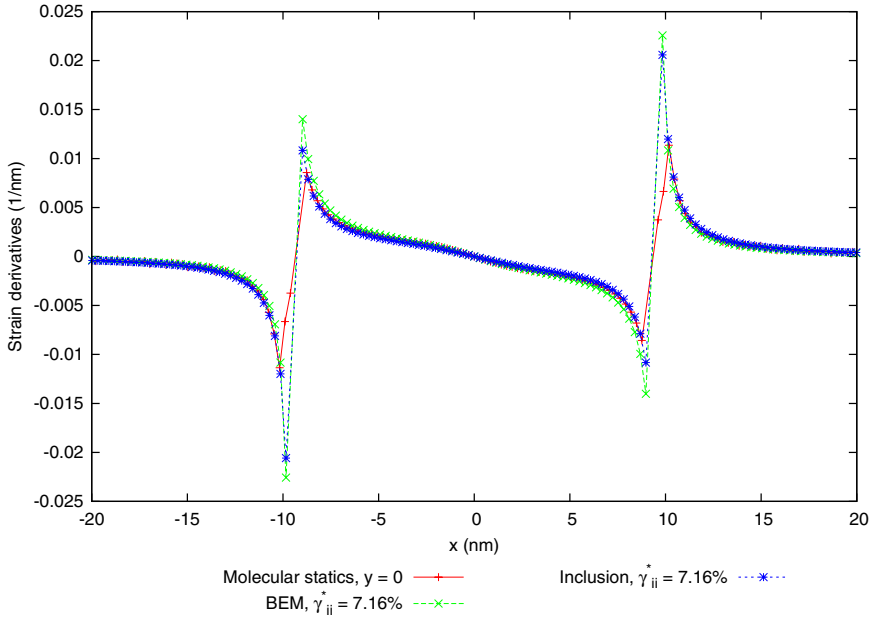

Figure 12. Strain derivative $\epsilon_{13,3}$ for points along the diagonal line $x = z$.

Acknowledgments

This work was supported by the Defense Threat Reduction Agency Joint Science and Technology Office (DTRA-JSTO) under the grant W911NF-06-2-0038. Also, while the final molecular statics calculations were done on our own PCs, preliminary molecular statics calculations were supported in part by an allocation of computing time from the Ohio Supercomputing Center.

References

[1] Dettmer R 1988 *IEE Rev.* **34** 395–7
[2] Makeev M A and Madhukar A 2002 *App. Phys. Lett.* **81** 3789–91
[3] Migliorato M A, Cullis A G, Fearn M and Jefferson J H 2002 *Phys. Rev.* B **65** 115316
[4] Eaglesham D J and Cerullo M 1990 *Phys. Rev. Lett.* **64** 1943–6
[5] Pan E, Han F and Albrecht J D 2005 *J. Appl. Phys.* **98** 013534
[6] Pan E 2004 *J. Mech. Phys. Solids* **52** 567–89
[7] Han F, Pan E and Albrecht J D 2006 *Superlatt. Microstruct.* **40** 125–36
[8] Madelung O (ed) 1996 *Semiconductors—Basic Data* 2nd edn (Berlin: Springer)
[9] Pryor C, Kim J, Wang L W, Williamson A J and Zunger A 1998 *J. Appl. Phys.* **83** 2548–54
[10] Keating P N 1966 *Phys. Rev.* **145** 637–45
[11] Martins J L and Zunger A 1984 *Phys. Rev.* B **30** 6217–20
[12] Kikuchi Y, Sugii H and Shintani K 2001 *J. Appl. Phys.* **89** 1191–6
[13] Tersoff J 1989 *Phys. Rev.* B **39** 5566–8
[14] Tersoff J 1988 *Phys. Rev.* B **38** 9902–5
[15] Sayed M, Jefferson J H, Walker A B and Cullis A G 1995 *Nucl. Instrum. Methods Phys. Res.* B **102** 218–22
[16] Smith R 1992 *Nucl. Instrum. Methods Phys. Res.* B **67** 335–9
[17] Ashu P A, Jefferson J H, Cullis A G, Hagston W E and Whitehouse C R 1995 *J. Cryst. Growth* **150** 176–9
[18] Plimpton S J 1995 *J. Comput. Phys.* **117** 1–19 http://lammps.sandia.gov/
[19] Sandia National Laboratories 2008 *LAMMPS Documentation* Latest version available online from http://lammps.sandia.gov/doc/Manual.html
[20] Horstemeyer M F and Baskes M I 2000 *Multiscale Phenomena in Materials—Experiments and Modeling* vol 578, ed I M Robertson, D H Lassila, B Devincre and R Phillips (Washington, DC: Materials Research Society) pp 15–20
[21] Gannepalli A and Mallapragada S K 2002 *Phys. Rev.* B **66** 104103
[22] Li J and Shimizu F, Least-square atomic strain available from http://alum.mit.edu/www/liju99/Graphics/A/annotate_atomic_strain/Doc/main.pdf This is a description of the algorithm behind the strain tensor calculations in AtomEye [23].
[23] Li J 2003 *Modelling Simul. Mater. Sci. Eng.* **11** 173–7
[24] Steinmann P, Elizondo A and Sunyk R 2007 *Modelling Simul. Mater. Sci. Eng.* **15** S271–81
[25] Mase G T and Mase G E 1999 *Continuum Mechanics for Engineers* 2nd edn (Boca Raton, FL: CRC Press)
[26] Clyne T W 1993 *An Introduction to Metal Matrix Composites* (Cambridge: Cambridge University Press)
[27] Paladugu M, Zou J, Wang H, Auchterlonie G J, Kim Y, Joyce H J, Gao Q, Tan H H and Jagadish C 2006 *Int. Conf. on Nanosci. and Nanotech.* (Piscataway, NJ: IEEE) pp 600–3
[28] Guo W, Guico R S, Xu J M and Beresford R 2007 *J. Vac. Sci. Technol.* B **25** 1072–6
[29] Brebbia C A and Dominguez J 1992 *Boundary Elements: an Introductory Course* (Southampton: WIT Press)
[30] Ting T C T 1996 *Anisotropic Elasticity* (Oxford: Oxford Science)
[31] Mura T 1987 *Micromechanics of Defects in Solids* 2nd edn (Dordrecht: Martinus Nijhoff)
[32] Faux D A, Downes J R and O'Reilly E P 1997 *J. Appl. Phys.* **82** 3754–62
[33] Keyes R W 1962 *J. Appl. Phys.* **33** 3371–2
[34] Ellaway S W and Faux D A 2002 *J. Appl. Phys.* **92** 3027–33